Isı Bilimi ve Tekniği Dergisi, 40, 1, 53-63, 2020
J. of Thermal Science and Technology

ISSN 1300-3615

VALIDATION OF AERODYNAMIC HEATING PREDICTION TOOL

Buğra ŞİMŞEK*, Sıtkı USLU and Mehmet Ali AK*****
*,**TOBB Ekonomi ve Teknoloji Üniversitesi, Söğütözü Caddesi No:43, 06560, Ankara,
*bsimsek@etu.edu.tr, **suslu@etu.edu.tr
*** ROKETSAN AŞ., Kemalpaşa Mah. Şehit Yüzbaşı Adem Kutlu Sk. No:21, 06780, Ankara, mehmetali.ak@roketsan.com.tr

(Geliş Tarihi: 03.02.2019, Kabul Tarihi: 22.01.2020)

Abstract: Validation of one-dimensional aerodynamic heating and ablation prediction program, *AeroheataBS* to calculate transient skin temperatures and heat fluxes for high-speed vehicles has been performed. In the tool shock relations, flat plate convective heating expressions, Eckert's reference temperature method and modified Newtonian flow theory are utilized to compute local heat transfer coefficients. Corresponding governing equations are discretized explicitly and numerically solved. Time varying flight conditions including velocity, altitude and angle of attack serve as input to the program. In order to examine the accuracy of aerodynamic heating capabilities of *AeroheataBS*, calculated temperature histories are compared with flight data of the X-15 research vehicle, a modified von-Karman nose shaped body, cone-cylinder-flare configuration and results of conjugate computational fluid dynamics studies. Comparative studies show that computed values are in good agreement with the reference data and prove that methodology established in *AeroheataBS* is appropriate for estimating aerodynamic heating and structural thermal response.
Keywords: Aerodynamic heating, thermal design of missiles, thermal protection systems.

AERODİNAMİK ISINMA KESTİRİM ARACININ DOĞRULANMASI

Özet: Yüksek hızlı hava araçlarının gövde sıcaklıklarını ve aerodinamik ısı akılarını hesaplama yazılımı olan, bir boyutlu aerodinamik ısınma ve ısıl aşınma kestirim yazılımı, *AeroheataBS*'in doğrulama çalışmaları yürütülmüştür. Şok denklemleri, düz plaka üzeri taşınım ısı transferi yaklaşımları, Eckert'in referans sıcaklık yöntemi ve değiştirilmiş Newton yasası aerodinamik ısınmanın hesaplanmasında kullanılmıştır. Denklemler açık olarak ayrıklaştırılmış ve sayısal olarak çözülmüştür. Işınım ile olan ısı transferi de dikkate alınmıştır. Uçuş hızı, uçuş irtifası ve hücum açısı zamana bağlı olarak tanımlanmıştır. Hesaplamaların doğruluğu literatürde bulunan uçuş verileriyle ve hesaplamalı akışkanlar dinamiği çalışmalarının sonuçlarıyla kıyaslanarak değerlendirilmiştir. Kıyaslamalarda gözlemlenen uyumlu sonuçlar *AeroheataBS* yazılımında kullanılan yöntemin aerodinamik ısınmanın ve gövde sıcaklıklarının kestiriminde kullanılabileceğini göstermiştir.
Anahtar kelimeler: Aerodinamik ısınma, füzelerin ısıl tasarımı, ısıl koruma sistemleri.

NOMENCLATURE

c_p	Specific heat [J/kgK]
h	Heat transfer coefficient [W/m^{2}K]
k	Thermal conductivity [W/mK]
M_L	Local Mach number [-]
M_∞	Free stream Mach number [-]
Nu_x	Nusselt number at point x [=hx/k]
P_L	Local pressure [Pa]
Pr	Prandtl number [=μc_p/k]
P_{0L}	Local stagnation pressure [Pa]
q''_{hw}	Hot wall heat flux [W/m^2]
Re_x	Reynolds number at point x [=Vρx/μ]
r	Recovery factor
$\dot{s}$	Surface recession rate [m/s]
St	Stanton number [h/ρc_pV]
t	Time [s]
T	Temperature [K]
T_L	Local temperature [K]
T_r	Recovery temperature [K]
T_w	Wall temperature [K]
T*	Eckert's reference temperature [K]
T_0	Total temperature [K]
T_∞	Free stream temperature [K]
V_l	Local velocity [m/s]
v	Volume [m^3]
y	Distance along thickness direction [m]
α	Thermal diffusivity [m^2/s]
γ	Specific heat ratio [-]
Δy	Mesh size [m]
Δt	Time step size [s]
δ	Thickness [m]
ε	Emissivity [-]
η	Blowing coefficient [-]
μ	Viscosity [Pa s]
ρ	Density [kg/m^3]
σ	Stefan-Boltzman constant [W/m^{2}K^4]

INTRODUCTION

Aerodynamic heating is conversion of kinetic energy into heat energy due to relative motion between a body and flow and the subsequent transfer of this energy to the skin and the interior of the body. Some portion of heat is

produced by compression of fluid across the shock near the stagnation regions and additional heat results from viscous dissipation inside the boundary layer.

Aerodynamic heating is one of the major concerns in the design of high-speed vehicles since success of mission strongly depends on surviving in harsh thermal environment. Thermal protection systems are used to maintain the underlying structure and avionics within allowable temperature limits. Selection of an appropriate thermal protection system is highly bound to accuracy of the thermal environment estimation since poor estimation leads poor design and mission failure. Therefore preliminary thermal design of high speed vehicles requires precisely and reliably predicting the convective heating over the vehicle. Detailed reviews about the advances made within the past 50 years of aerodynamic heating and thermal protection systems can be found in Bertin and Cummings (2003). Analytical calculations for aerodynamic heating are available under certain conditions and assumptions. The work (Liu and Cao, 2017) deals with how to use suitable equations of convective heat transfer coefficient to compute aerodynamic heating in high speed laminar flow over a flat plate under incoming flow Mach numbers 1 to 10. Another detailed analytical study of the aerodynamic heating problem for both laminar and turbulent flow regimes is given in Arnas et al., (2010). In that study by use of Newton's second law of motion, continuity equation, first law of thermodynamics and the equation of state, governing equations are derived and appropriate aerodynamic heat transfer equations are developed. Additional methods of predicting aerodynamic heating to blunt-nosed bodies, flat plates and sharp cones through the hypersonic speed range for laminar, transitional or turbulent boundary layers are described in Crabtree et al., (1970). Comparisons of some engineering correlations to predict aerodynamic heating with CFD results and experimental data are published in Higgins (2005). Good agreement was observed between the results obtained from laminar correlations, CFD simulations and experimental data. Comparisons of turbulent correlation results with CFD and experimental data produced reasonable agreement in most cases. Aerodynamic heating can be estimated by following three different ways which are ground testing, numerical simulation and approximate engineering methods (Yang et al., 2014). One of the major difficulties with ground testing is to generate exact flight conditions and to determine the suitable testing configuration. Verification of the test facility, providing the required test conditions, is also challenging (Mazaheri et al., 2014). Therefore, it is hard to determine exactly which parameters must be reproduced and how the ground to flight connection must be done. In addition, ground testings are generally costly compared to other methods.

Developments in Computational Fluid Dynamics, CFD make numerical computations the best to predict aerodynamic heating. Computer power makes it possible to solve the most of the complex equations numerically for many different types of designs and flight trajectories of interest; unfortunately, complicated methodologies of CFD include some difficulties. Intense modeling efforts should be made to improve the level of accuracy and too much computational time may be required to calculate complete time histories of transient temperature and heat flux. It is not appropriate for the early phases of design, which requires for predictions and design iterations to provide proof of concept for new vehicles. There are many studies reported in the literature for the calculation of aerodynamic heating using CFD simulations. In Barth (2007), aerothermodynamic analysis of the flight of SHEFEX 1 is presented. By use of in-house CFD solver, Navier-Stokes computations have been performed to compare the numerical results with the experimental data. Well agreement between the numerical and experimental data is seen for selected altitudes of the trajectory. CFD analysis of HYFLEX (Hypersonic Flight Experiment) is published in Murakami et al., (2004). In this study temperature history of the nose cap is evaluated and compared with the available flight data. CFD analysis of the post flight wind tunnel experiments are also conducted for the comparison studies.

Approximate engineering methods can be followed to obtain rapid predictions with their reasonable accuracy and much less running times compared to multi-dimensional numerical simulations. These estimations are performed to determine the seriousness of the problem and identify the most critical conditions of flight. Many engineering estimation tools have been developed to compute aerodynamic heating such as AEROHEAT (Quinn and Gong, 1990), MINIVER (Louderback, 2013), TPATH (Quinn and Gong, 2000), INCHES (Hamilton et al., 1993), LATCH (Hamilton et al., 1994), HABP (Smyth and Loo, 1981), CBAERO (Kinney, 2004) and HATLAP (Jain and Hayes, 2004).

Each of these codes uses different types of methods for aerodynamic heating. Unfortunately, tools are allowed for in-house use only and most of them are subject to export control regulations and are not commercially available.

Aerodynamic heating and ablation simulation software, *AeroheataBS* has been developed to compute transient structural thermal response. Flight parameters including velocity, height and angle of attack are utilized to find the convective boundary conditions. Both laminar and turbulent flows have been considered. Compressibility effects are taken into account by reference temperature method. Material properties are used as a function of temperature. All of the input parameters are defined by developed graphical user interface, GUI of the software.

In the present work, verification studies for aerodynamic heating capabilities of *AeroheataBS* are presented. Verification of ablation, remeshing capabilities and numerical approaches of the code is out of scope and can be found in Simsek and Uslu (2019).

MATHEMATICAL BACKGROUND

Governing Equations

Insulation and underlying structure have been divided by a network of nodes and governing equations are derived from rate based general form of conservation of energy given in Eq. (1) for each element about the assigned node.

$$\dot{\mathrm{E}}_{\mathrm{in}} - \dot{\mathrm{E}}_{\mathrm{out}} = \dot{\mathrm{E}}_{\mathrm{st}} \quad (1)$$

The energy inflow, $\dot{\mathrm{E}}_{\mathrm{in}}$ and outflow term, $\dot{\mathrm{E}}_{\mathrm{out}}$ for the element boundaries are substituted with conduction rate equations given in Eq. (2). Energy storage term, $\dot{\mathrm{E}}_{\mathrm{st}}$ is calculated as given in Eq. (3).

$$q" = -k\left(\frac{\partial T}{\partial y}\right) \quad (2)$$

$$\dot{E}_{st} = \mathrm{v}\rho c_p\left(\frac{\partial T}{\partial t}\right) \quad (3)$$

Points away from the stagnation regions are exposed to aerodynamic heating due to viscous dissipation inside the boundary layer. Computation of temperature response of the structure has been carried out setting incident heat flux as given in Eq. (4). Equation (4) shows that aerodynamic heating is directly proportional to the difference between the recovery temperature and the wall temperature.

$$q_{hw}^{"} = -k\left(\frac{\partial T}{\partial y}\right)_{y=\delta} = \eta h(T_r - T_w) - \sigma\varepsilon(T_w^4 - T_\infty^4) \quad (4)$$

In Eqn (4), η is the blowing coefficient that accounts the ablation effects on heat transfer coefficient. Recovery temperature, also known as adiabatic wall temperature, is calculated as given in Eq. (5). The recovery temperature is the upper limit for the surface temperature and when it is reached, no exchange of heat takes place between the flow and the wall. The adiabatic wall temperature is higher than the freestream temperature and "drives" the convective aerodynamic heating.

$$T_r = T_L\left(1 + r\frac{\gamma - 1}{2}M_L^2\right) \quad (5)$$

The recovery factor, *r* depends on flow type. It is estimated as $\sqrt{\mathrm{Pr}}$ and $\sqrt[3]{\mathrm{Pr}}$ for laminar and turbulent flows, respectively (Bertin, 1994). For viscous flow over a body, the local Mach number and the local temperature can be predicted using inviscid isentropic relations. The relationship between the local Mach number and the local static pressure is given in Eq. (6). Isentropic formulation for the local temperature as a function of the local Mach number and the total temperature is given in Eq. (7).

$$M_L = \sqrt{\left[\left(\frac{P_{0L}}{P_L}\right)^{\frac{\gamma-1}{\gamma}} - 1\right]\frac{2}{\gamma - 1}} \quad (6)$$

$$T_L = T_0 / \left(1 + \frac{\gamma - 1}{2}M_L^2\right) \quad (7)$$

For subsonic speeds, the local stagnation pressure can be calculated using a simple isentropic relation. For supersonic speeds, it is found using normal shock wave equations with the assumption of bow shock behaving similar to a normal shock at the center in the transverse direction. The total temperature is constant across a normal shock wave for the adiabatic flow of a perfect gas and it is found by Eq. (8).

$$T_0 = T_\infty\left(1 + \frac{\gamma - 1}{2}M_\infty^2\right) \quad (8)$$

Local static pressure is calculated by use of Modified Newtonian theory. The Newtonian theory assumes that when flow strikes a surface, the normal component of momentum to that surface diminishes and the freestream flow moves along the surface with its tangential component of momentum unchanged (Hankey, 1988). This theory is valid for the estimation of local static pressure over all surfaces experiencing non-separated flows. In modified theory, pressure coefficient is corrected by use of the maximum value of the pressure coefficient, evaluated at a stagnation point behind a normal shock wave. For the prediction of pressure distribution over blunt-nosed bodies, Modified Newtonian theory yields in considerably more accurate results than does the straight Newtonian theory (Anderson, 2006). Modified Newtonian theory is also attractive because it requires only the angle between the freestream velocity vector and the inward normal to the surface. Theoretical background of the modified Newtonian theory is published in Lees (1955). Flow phenomena which give rise to significant differences between the actual pressures and those predicted using modified Newtonian flow are described in Bertin (1994). Examples of where such differences seen are (Bertin 1994):

- In the flow behind the shock-wave of a truncated blunt body.
- In the rapid overexpansion and recompression of the flow around the nose region of a sphere.
- On the control surfaces/wings where additional shock waves are seen within the shock layer.

In general, Newtonian theory provides satisfactory results when Mach number is large and/or the flow deflection angle is large (Bertin, 1994). Its use at subsonic and low supersonic speeds is justified by the continuity and simplicity it provides in the lower Mach number regions where aerodynamic heating rates are negligible. Effects of the angle of attack and surface conical angle on the aerodynamic heating are taken into account by the modified Newtonian theory since angle between the flow direction and surface normal is used to find its tangential and normal components.

Free stream properties are estimated by interpolating the 1976 U.S. Standard Atmosphere model versus the altitude. Nusselt numbers for laminar and turbulent flows are expressed below, respectively (Arnas et al., 2010).

$$Nu_x = 0.332\sqrt{Re_x}(Pr)^{\frac{1}{3}} \quad (9)$$

$$Nu_x = 0.0291(Re_x)^{\frac{4}{5}}(Pr)^{\frac{1}{3}} \quad (10)$$

Three-dimensional relieving effects make the boundary layer thinner for the cone. This in turn results in larger velocity and temperature gradient in the boundary layer and hence causes a higher heat transfer and skin friction than in the two-dimensional boundary layer over a flat plate (Anderson, 2006). For the conical side of the body, heat transfer coefficient, h is multiplied by the Mangler fraction $\sqrt{3}$ and then computation is made as for a flat plate (Crabtree et al., 1970). Derivation of the factor $\sqrt{3}$ can be found in both Anderson (2006), Hantzsche and Wendt (1947). By use of this factor, relation between the Nusselt number for conical and planar regions is given in Eq. (11) for laminar flows.

$$Nu_{x,conical} = \sqrt{3}Nu_{x,planar} \quad (11)$$

Thermodynamic and transport properties are found at Eckert's reference temperature, T* which is given in Eq. (12). Eckert's reference temperature method is used to add compressibility effects into the convectional heat transfer equations. The reference temperature method provides a simple engineering approach to calculating the surface skin-friction and aerodynamic heating for compressible boundary layers using classic results from incompressible flow (Anderson, 2006). Recently, Meador and Smart (2005) suggested improved equations for the calculation of the reference temperature for laminar and turbulent flows.

$$T^* = T_L + 0.5(T_w - T_L) + 0.22(T_r - T_L) \quad (12)$$

Thermal conductivity, density, dynamic viscosity and specific heat of air are computed at reference temperature. Sutherland equations which are given in Eq. (13) and Eq. (14) are used to determine the dynamic viscosity and the thermal conductivity, respectively. In these equations temperature is given in K, viscosity in kg/m.s and thermal conductivity in W/m K.

$$\mu = 1.458x10^{-6}\frac{T^{1.5}}{T + 110.4} \quad (13)$$

$$k = 1.993x10^{-3}\frac{T^{1.5}}{T + 112} \quad (14)$$

Finally, Nusselt number for laminar and turbulent flow conditions can now be written as in Eq. (15) and Eq. (16), respectively. Heat transfer coefficient, h is then evaluated from the given Nusselt number correlations. In the equations, superscript (*) indicates that corresponding property is calculated at the reference temperature.

$$Nu_x^* = \frac{hx}{k^*} = 0.332\sqrt{\frac{\rho^* V_l x}{\mu^*}}\left(\frac{\mu^* c_p^*}{k^*}\right)^{\frac{1}{3}} \quad (15)$$

$$Nu_x^* = \frac{hx}{k^*} = 0.0291\left(\frac{\rho^* V_l x}{\mu^*}\right)^{\frac{4}{5}}\left(\frac{\mu^* c_p^*}{k^*}\right)^{\frac{1}{3}} \quad (16)$$

Following the calculation of heat transfer coefficient, convective heat flux is evaluated at each time step by use of Eq. (4). Temperature distribution along the wall is then determined by use of boundary conditions and explicit finite difference equations derived for interior nodes.

In Eq. (4) η is the reduction of the heating due to mass injection into boundary layer. This phenomenon thickens the boundary layer and causes a decrease in aerodynamic heating (Bianchi, 2007). Reduction rate is estimated by a simple relation expressed in Eq. (17).

$$\eta = \frac{\Phi}{e^{\Phi} - 1} \quad (17)$$

In Eqn. (17), Φ is a function of mass injection rate, local flow density, local velocity and unblown Stanton number. Pyrolysis gas flux is calculated by use of conservation of mass for each node by considering density change due to decomposition. Mass loss rate due to ablation is approximated by use of surface recession. Decomposition of insulation is modeled by Arrhenius relation and steady state ablation approach employing heat of ablation is performed to predict surface recession.

In previous work, verification of finite difference computations are made by use of analytical solutions of transient conduction, transient conduction with convection and transient conduction with temperature dependent material properties. It was shown that 0.1 mm mesh size and 0.001 s time step size are appropriate to attain the required accuracy. In Simsek and Uslu, (2019) code-to-code comparison is also performed using MSC MARC for an ablation problem with specified surface recession. It is showed that newly developed prediction tool can also be used for problems where the surface recession is known. Thermochemical ablation model is verified using arcjet test results of a low-density phenolic impregnated carbon ablator (PICA). The computed and experimental surface temperatures show reasonable agreement with a maximum discrepancy of approximately 10%. Details of the decomposition and surface recession are out of scope of this study and details can be found in Simsek and Uslu, (2019).

Laminar to turbulent transition criteria recommended by Quinn and Gong (2000) is implemented into the tool. In the criteria, transition Reynolds number is a function of local Reynolds number and local Mach number. Different types of transition models are also implemented into tool and selection of the model is left to the user. Fully turbulent and laminar computations without transition are also possible.

Developed methodology has the following limitations.

- In *AeroHeataBS*, aerodynamic heating due to skin friction is computed. Locations close to the stagnation regions such as leading edges of wings and tips of nose cones cannot be computed by this methodology. Work to develop a methodology for stagnation point heating is currently going on.
- In the current methodology, perfect gas assumption is made. At hypersonic speeds dissociation and ionization of air takes place and specific heat ratio of air cannot be assumed as constant any longer. Implementation of real gas effects into *AeroheataBS* is being studied.
- Due to one-dimensional computation, complex geometries and longitudinal conduction effects are not considered. Shock/boundary-layer interaction cannot be simulated by *AeroheataBS.*
- Several problems in which flow separation occur. A consequence of flow separation is to increase significantly the local aerodynamic heating.

FINITE DIFFERENCE APPROACH

Thickness of the missile wall is divided into elements by nodal network with constant mesh size, Δy normal to flow direction. Each of the interior nodes is centered at the elements. Surface and back-face nodes are assigned a thickness that is one-half that of the interior nodes. Longitudinal conduction in the missile wall is neglected since temperature gradients in that direction are much smaller than in the normal radial direction except near the leading edge nose. Circumferential velocity and pressure gradients are also neglected in the *AeroheataBS*. Detailed 3-D CFD simulations are required to capture these effects on the aerodynamic heating especially in the cases with high yaw angles.

In the preliminary design phase, neglecting 3-D effects are acceptable for rapid predictions. Representation of the discretized wall is illustrated in Fig.1.

Governing equations are discretized explicitly for each node assigned to each element. Explicit means that temperature computations at each node for a future time are based on the present values at the node and its neighbors. If the temperature distribution at an initial time is known, the distribution at a future time can be computed (Chapra and Canale, 2015). To illustrate the methodology, discretized governing equation for i=3 is given in Eq. (18) which is obtained from the energy balance equation. The first term represents the energy flux from the 2nd element to the 3rd element by conduction. Similarly, the second term in the equation shows the energy flux from the 3rd element to the 4th element by conduction. Term on the right hand side is the energy storage in the third element. For each grid point, governing equations are derived and solved explicitly to calculate nodal temperatures for each instant of time. For the surface node, energy inlet term is calculated by convection and radiation which is given in Eq. (4).

$$[k_2(T_2^n)]\frac{T_2^n - T_3^n}{\Delta y^n} - [k_3(T_3^n)]\frac{T_3^n - T_4^n}{\Delta y^n} = \Delta y^n[\rho_3(T_3^n)][c_{P3}(T_3^n)]\frac{T_3^{n+1} - T_3^n}{\Delta t} \quad (18)$$

Insulation thickness and mesh size are updated as shown in Eq. (19) and Eq. (20) respectively for each time step. In Eqn. (20), N is the total number of nodes.

$$\delta^{n+1} = \delta^n - \dot{s}^n \Delta t \quad (19)$$

$$\Delta y^{n+1} = \frac{\delta^{n+1}}{N-1} \quad (20)$$

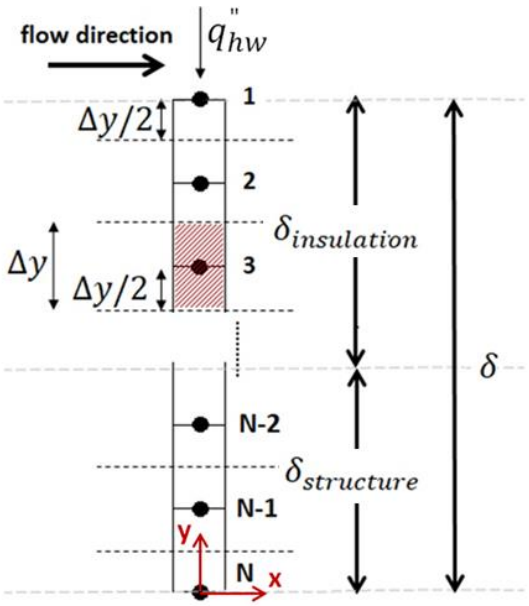

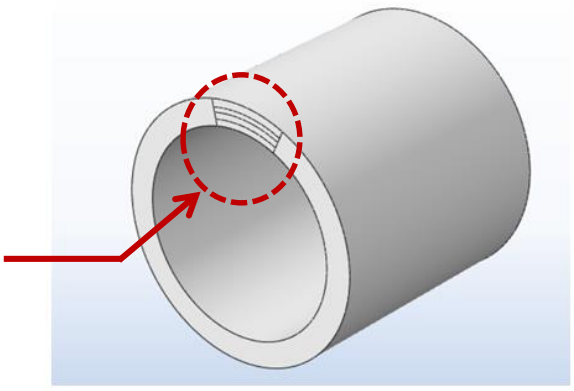

Figure 1. Schematic representation of solution domain

Explicit discretization is 'conditionally' stable. Solution may present numerically induced oscillations, which are physically impossible. These oscillations may cause divergence. To avoid divergence, time step size should be less than a certain limit. By use of stability criteria which is given in Eq. (21), certain limit value for the time step size can be calculated by Eq. (22).

$$\left(1 - 2\frac{\alpha \Delta t}{\Delta y^2}\right) \geq 0 \tag{21}$$

$$\Delta t \leq \frac{1}{2}\frac{\Delta y^2}{\alpha} \tag{22}$$

During computations, if the stability criterion is not satisfied, computation is terminated with an error message. In Simsek and Uslu (2019), detailed comparison studies for different mesh and time step sizes are investigated and as a rule of thumb a time step size of 0.001 seconds is recommended for missile applications.

Due to stability concerns recommended minimum mesh sizes for some material types are given in
Table 1 for Δt=0.001 s. In general, in order to increase the accuracy, mesh and time step sizes should be as small as possible.

Table 1. Recommended minimum mesh sizes for different material types.

Material Type	k (W/mK)	c_p (J/kgK)	ρ (kg/m^3)	Δx (mm)
Inconel	12	431	8280	0.082
Aluminum	167	896	2700	0.371
Steel	42	473	7700	0.152
Insulation	0.2	1500	1200	0.015

STRUCTURE OF *AeroheataBS*

AeroheataBS can be divided into several major sections. In the first section, input files including flight trajectory, material properties, standard atmosphere data, initial conditions and geometric properties are imported from external files. Total number of nodes and time step size are also defined in this section. In the second section, free stream properties are calculated by use of standard atmosphere model. Recovery temperature, dynamic pressure and local flow properties are also computed. In the third section, Eckert's reference temperature and corresponding Reynolds number are calculated. Type of flow regime is determined in this section. Temperature distribution along the thickness is calculated in the fourth section. Ablation parameters including surface recession and blowing ratio are computed in the next section. Thickness of the insulation is updated for the following time step. Calculations continue until the total flight duration is reached. In the last section, all of requested parameters are written in text file and surface temperature histories are plotted. The flow logic used in the *AeroheataBS* is illustrated in Fig.2.

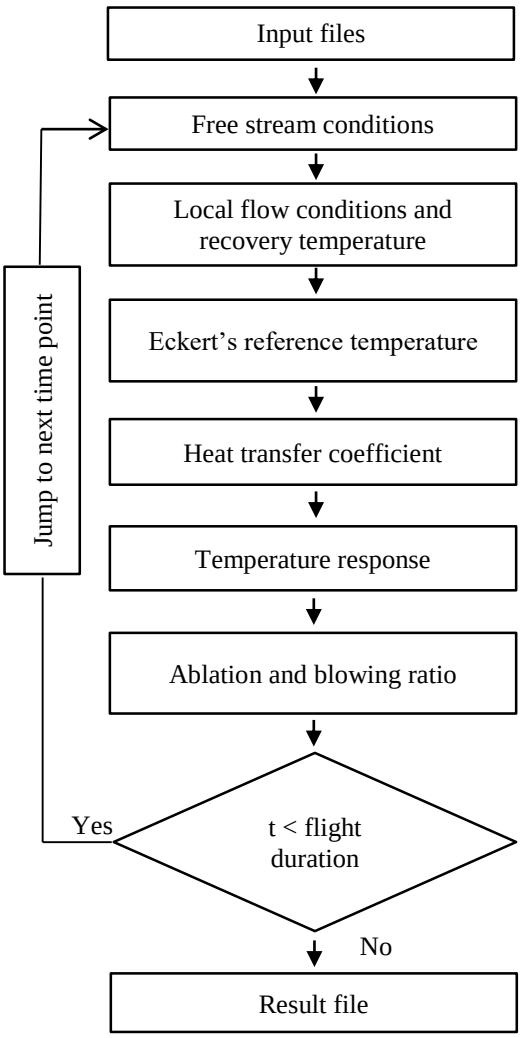

Figure 2. Flowchart of *AeroheataBS*

VALIDATION OF THE TOOL

In order to validate the accuracy of the *AeroheataBS*, four different cases are examined. The following assumptions are made in all of the cases:

- Air is assumed to be a perfect gas; γ is constant and equal to 1.4.
- Properties of the structural material are constant and used as given in corresponding reference study.
- Time step size is 0.001 s. for all cases. For the first and second case, mesh size is 0.1 mm, for the third and fourth case mesh size is 0.5 mm.
- An adiabatic condition is applied to the bottom wall, not exposed to the aerodynamic heating.
- Longitudinal heat conduction is neglected since thermal gradient is larger in radial direction compared to longitudinal direction.

The first data belongs to a modified Von-Karman nose shaped body. The body which consisted of a modified fineness ratio 5, von Karman nose shape, a fineness ratio 5 cylinder and a frustum of a cone is shown as a sketch in Fig.3 (William and Katherine, 1961).

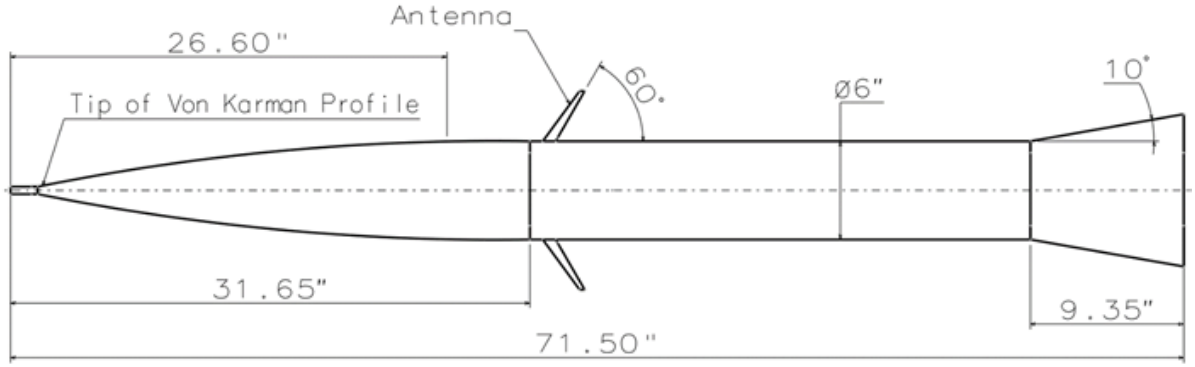

Figure 3. Sketch of model with dimensions (inches) (William and Katherine, 1961).

Mathematically, fineness ratio is the ratio of the length of a body to its maximum diameter. The body is 0.8128-mm-thick (0.032 inches) Inconel. Temperature measurement point is 675.6 mm (26.6 inches) behind the nose tip. Flight trajectory is digitized from William and Katherine (1961) and is given in Fig.4. As can be seen from the velocity profile, system has four stages. After nearly 15 s. the first stage burns out and the second stage is ignited. Third stage is ignited at 22 seconds and the fourth stage is ignited at 31 seconds. Two different cases, fully turbulent and transitional with specified Reynolds number are computed with *AeroheataBS* and results are compared in Fig.5. Prediction of Wing (1971) is also included in comparison.

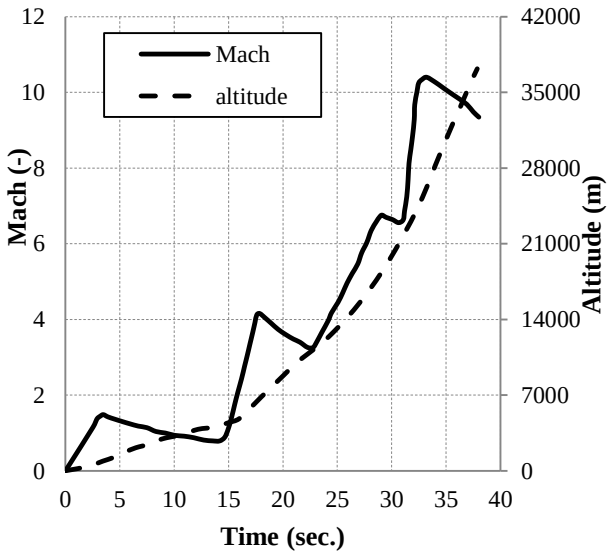

Figure 4. The histories of the velocity and altitude (William and Katherine, 1961).

As seen in Fig.5, the calculated results are followed the experimental data and predictions done by Wing (1970) closely during the first 30 s. From this point on, agreement between *AeroheataBS*, referenced prediction and flight data agreed best when transition local Reynolds number of ten million; indicating relaminarization from turbulent to laminar flow probably occurred at this local Reynolds number.

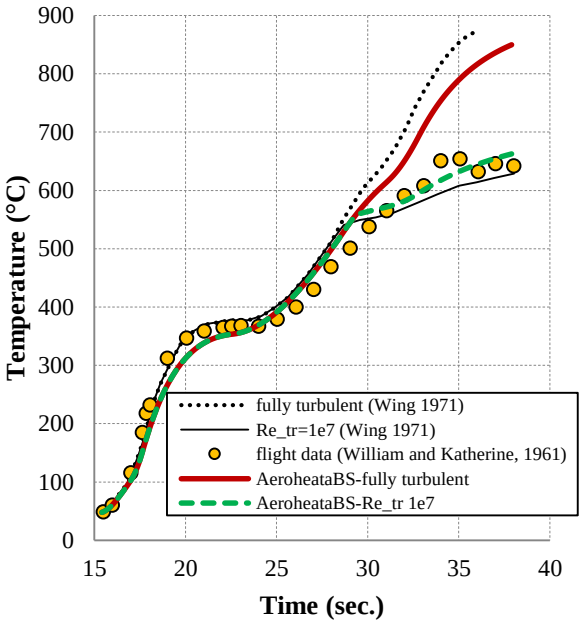

Figure 5. Comparison of *AeroheataBS* with flight data and another code prediction.

Numerous flow field parameters, including surface roughness, wall temperature, mass injection into boundary layer due to ablation, gas chemistry etc. affect transition from laminar to turbulent flow. Premature transition may occur due to unpredictable events and increase heat loads. For a safe-side estimation of aerodynamic heating, it is desirable to consider the fully turbulent flow in thermal design. Fully turbulent solution of *AeroheataBS* also agrees well with the fully turbulent solution of the Wing (1970) and the maximum discrepancy is less than 7%.

The second part of the comparative study includes aerodynamic heating data of a 15° cone-cylinder-flare configuration in flight up to 4.7 Mach (Rumsey and Lee, 1958). The conical nose has a total angle of 15° and is 31 inches long. The cylindrical section was 8.5 inches in diameter and 35 inches long. The flare skirt, which provides aerodynamic stability, had a 10°half-angle and a base diameter of 15.55 inches. Total length of the model was 86 inches. Temperature history for a point which is

0.3556 m (14 inches) behind the nose tip, is calculated with *AeroheataBS* and results are compared with flight measured data and CFD studies presented by Charubhun and Chusilp (2017). Material of the skin is Inconel and thickness is 0.762 mm (0.03 inch). Reader is refered to Ramsey & Lee (1958) for model dimensions, parameters and measurement locations. Time histories of velocity and altitude are shown in Fig.6.

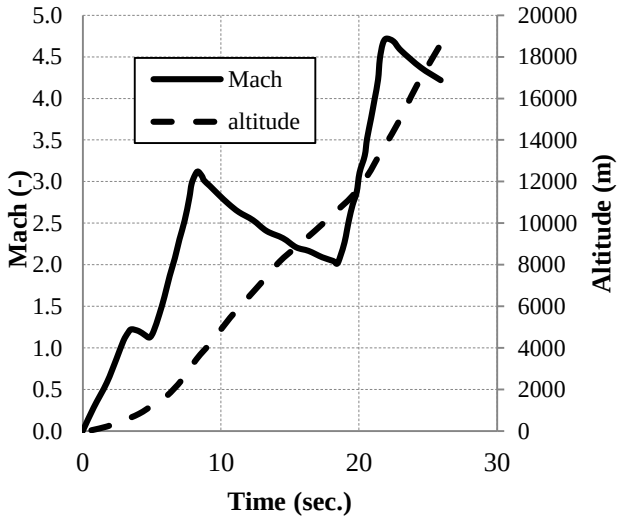

Figure 6. Digitized fligth profile from reference (Rumsey and Lee, 1958).

Results of *AeroheataBS* are compared with the flight data and results of the two-dimensional CFD simulations in which five turbulent models were utilized and effects of time step size on the results were investigated (Charubhun and Chusilp, 2017). Results of SST turbulence model are used for comparison as it showed best agreement with the flight data (Charubhun and Chusilp, 2017). As seen in Fig.7, predicted temperature histories agreed satisfactorily especially in the first 22 seconds of flight. Up to this point, computations overestimated the temperatures by about 30 °C. Discrepancy seen in the last three seconds may be the boundary layer transition. Near 22 seconds, an abrupt reduction in skin temperature of the flight data suggests relaminarization of the boundary-layer flow.

Temperature history predicted by *AeroheataBS* and by CFD simulations (Charubhun and Chusilp, 2017) show good agreement. According to Charubhun and Chusilp, (2017), total run time of a CFD analysis is 130 hours, however, run time of *AeroheataBS* for one benchmark point is less than 2 minutes. Although *AeroheataBS* calculates only for one point in a single simulation, timesaving advantage of *AeroheataBS* compared to CFD analysis is quite significant especially in early design stages in which complicated numerical computations may not be mandatory where computation for relatively small number of points seems to be sufficient. The striking advantage of the present approach would be lost if it is necessary to calculate the temperature for too many points which is in fact often not the case.

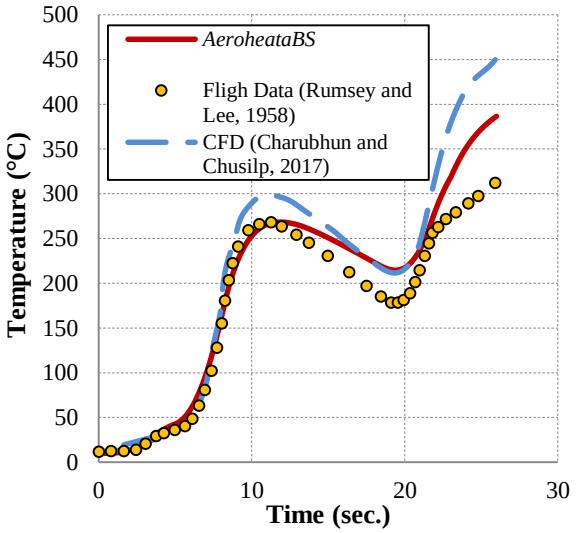

Figure 7. Comparison of the results and measured data.

Comparative studies are also performed with temperatures measured on the wing mid semi-span portion of X-15 plane at high-altitude flight and temperatures calculated by CFD studies presented in Hussain and Qureshi (2013). The flight trajectory is given in Fig.8. Angle of attack is digitized from same reference.

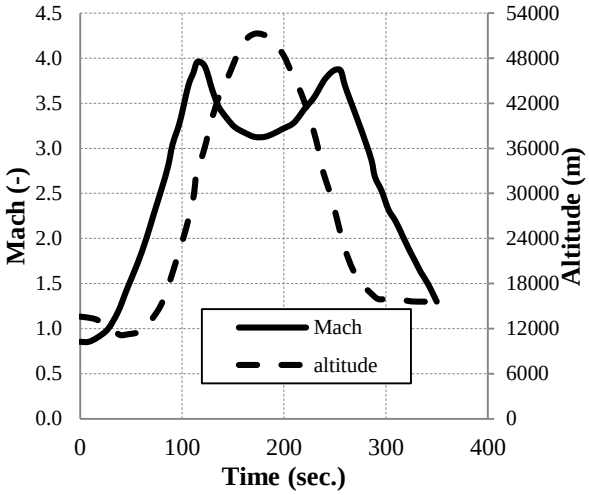

Figure 8. High-altitude flight profile.

Comparisons are made for two locations, at 4% and 20% windward side chord length. Thickness of the wing at points of interest is 1.44 mm (0.057 inch) and material is Inconel. Wing dimensions are obtained from Jenkins (2017). Two computations are made with *AeroheataBS* with different flow regime assumptions, fully turbulent and transition model recommended by Quinn and Gong (2000). Comparison of the results for the point located at %4 chord is given in Fig.9. As can be seen in Fig.9, a reasonably good agreement is captured between the CFD results and *AeroheataBS* predictions when no transition model is used. But when the laminar to turbulent transition is accounted for then an excellent agreement is obtained between the *AeroheataBS* predictions and the flight data. It is clear that flow in some parts of the flight is laminar since fully turbulent computations overestimate the measured flight data. Total run time of the

AeroheataBS simulation is 7 minutes. Fig.10 shows comparisons of measured and calculated temperatures on the point at 20% mid-span chord.

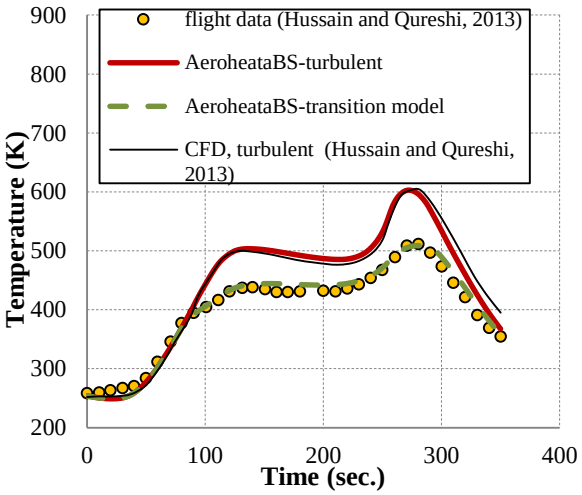

Figure 9. Comparison of measured and calculated temperatures, 4% chord.

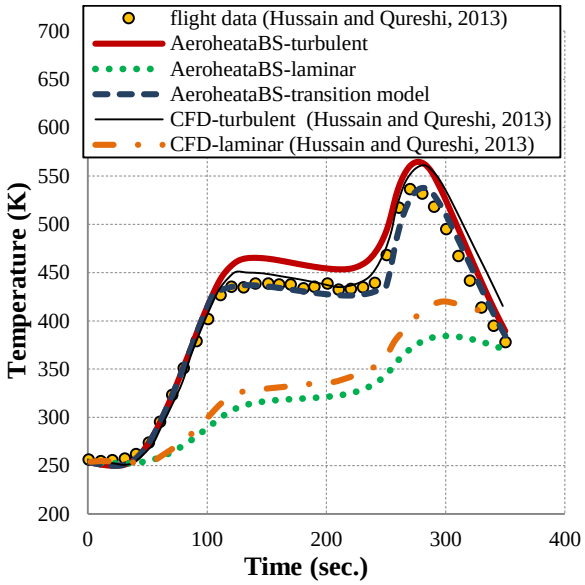

Figure 10. Comparison of measured and calculated surface temperatures at 20% chord.

Predicted temperature histories for turbulent and laminar conditions agree well with the CFD results as shown in Fig.10. The maximum discrepancies between the *AeroheataBS* and CFD results are 3% and 9% for turbulent and laminar flow regimes, respectively. Transition model of the *AeroheataBS* agrees excellent with the flight data. Fully laminar predictions underestimate the flight data, proving that turbulence is occurred during flight.

CONCLUSIONS

Validation studies of aerodynamic heating prediction tool, *AeroheataBS* to calculate transient in-depth temperature response have been described. Mathematical background and the working methodology of the tool are presented. Predicted transient surface temperatures are compared with the measured flight data and other available numerical results, which are published in the open literature. These comparisons show that the values predicted using the *AeroheataBS* are in good agreement with measured surface temperatures and CFD studies.

Different combinations of insulation and underlying material can be modeled over wide range of flight conditions. Fast prediction of aerodynamic heating under different flight conditions may help engineer to evaluate the alternatives of the options and to make the optimum design. Computed boundary conditions may also be exported to finite element solvers for detailed thermal analyses. Work to enhance capabilities of the *AeroheataBS* is going on.

REFERENCES

Anderson, J. D. Jr., 2006, *Hypersonic And High Temperature Gas Dynamics*, AIAA, Reston, VA, USA.

Arnas, A. Ö., D. D. Boettner, G. Tamm, S. A. Norberg, J. R. Whipple, M. J. Benson, and B. P. VanPoppel. 2010. On The Analysis Of The Aerodynamic Heating Problem. *J. Heat Transfer* 132 (12): 124501.

Barth T., 2007, Aero-Thermodynamic Analysis To SHEFEX I, *Engineering Applications of Computational Fluid Mechanics* Vol.1, No. 1.

Bertin, J. J., 1994, *Hypersonic Aerothermodynamics*, AIAA Education Series, AIAA, Reston, VA, USA.

Bertin, J. J., and R. M. Cummings, 2003. Fifty Years Of Hypersonics: Where We've Been, Where We're Going. *Prog. Aerosp. Sci.* 39 (6–7): 511–536.

Bianchi, D. , 2007, *Modeling Of Ablation Phenomena In Space Applications*, Ph.D. dissertation, Dept. of Mechanics and Aeronautics, The Sapienza University of Rome, Italy.

Chapra, S. C., and Canale R. P., 2015, *Numerical Methods For Engineers*, New York: McGraw-Hill Education.

Charubhun, W., and Chusilp P., 2017, Aerodynamic Heat Prediction On A 15 Degree Cone-Cylinder-Flare Configuration Using 2D Axisymmetric Viscous Transient CFD, *In Proc., 3rd Asian Conf. on Defense Technology*, Piscataway, NJ: IEEE.

Crabtree, L. F.,Woodley, J. G., and Dommett, R. L.,1970, Estimation of Heat Transfer to Flat Plates, Cones and Blunt Bodies, *Ministry of Technology, Aeronautical Research Council, Rept. and Memoranda* No. 3637, London.

Hamilton H. H., Greene F. A. and Dejarnette F. R., 1993, An Approximate Method For Calculating Heating Rates On Three-Dimensional Vehicles, AIAA paper 93-2881.

Hamilton, H. H., Greene, F. A., and DeJarnette, F. R., 1994, Approximate Method for Calculating Heating Rates on Three Dimensional Vehicles, *Journal of Spacecraft and Rockets*, Vol. 31, No. 3, 345-354.

Hankey W. L., 1988, *Re-Entry Aerodynamics*, AIAA Education Series, AIAA, Reston, VA, USA.

Hantzsche, W., and Wendt, H., 1947, The Laminar Boundary Layer on a Cone in a Supersonic Air Stream at Zero Angle of Attack, Jahrbuch 1941 der Deutschen Luftfahrtforschung. Also available as Translation No. RAT-6, Project RAND.

Higgins K., 2008, Comparison of Engineering Correlations for Predicting Heat Transfer in Zero-pressure-gradient Compressible Boundary Layers with CFD and Experimental Data, *Australia Defense Science and Technology Organization*, DSTO–TR–2159.

Hussain M., Qureshi M.N., 2013, Prediction Of Transient Skin Temperature Of High Speed Vehicles Through CFD, *6th International Conference on Recent Advances in Space Technologies*,Istanbul, Turkey.

Jain, A.C., Hayes, J.R., 2004, Hypersonic Pressure, Skin-Friction, and Heat Transfer Distributions on Space Vehicles: Planar Bodies", *AIAA Journal* Vol. 42 No. 10, 2060-2068.

Jenkins D.R., 2017, *X-15: Extending the Frontiers of Flight*, NASA.

Kinney, D. J., 2004, Aero-Thermodynamics for Conceptual Design, *42nd AIAA Aerospace Sciences Meeting and Exhibit*, Reno, NV, USA.

Lees, L., 1955, Hypersonic Flow, *5th International Aeronautical Conference*, Los Angeles, Inst. of Aeronautical Sciences, New York, 241–276.

Louderback P.M., 2013, *A Software Upgrade Of The NASA Aeroheating Code "MINIVER"*, MSC Thesis, Florida Institute of Technology, USA.

Liu C.,Cao W., 2017, Study Of Predicting Aerodynamic Heating For Hypersonic Boundary Layer Flow Over A Flat Plate, *International Journal of Heat and Mass Transfer* 111, 1079-1086.

Mazaheri A., Bruce W.E., Mesick N.J. Sutton K., 2014, Methodology For Flight-Relevant Arc-Jet Testing Of Flexible Thermal Protection Systems, *Journal of Spacecraft and Rockets*, Vol.51 No.3.

Meador, W. E., and Smart, M. K., 2005, Reference Enthalpy Method Developed from Solutions of the Boundary Layer Equations, *AIAA Journal*, Vol. 43, No. 1, 135–139.

Murakami K.,Yamamoto Y.,Rouzand O., 2004, CFD Analysis Of Aerodynamic Heating For Hyflex High Enthalpy Flow Tests And Flight Conditions, *24th International Congress of the Aeronautical Sciences*, Yokohama, Japan.

Quinn R.D., Gong L., 1990, Real Time Aerodynamic Heating And Surface Temperature Calculations For Hypersonic Flight Simulation, *NASA Technical Memorandum 4222*.

Quinn, R. D., and Gong L., 2000, A Method For Calculating Transient Surface Temperatures And Surface Heating Rates For High-Speed Aircraft, *NASA/TP-2000-209034*, Washington, DC: NASA.

Rumsey C.B., Lee D.B., 1958, Measurements of aerodynamic heat transfer on a 15° cone-cylinder-flare configuration in free flight at Mach numbers up to 4.7., *NACA RM LJ57J10*.

Smyth, D. N. and Loo, H. C., 1981, Analysis of Static Pressure Data from 1/12-scale Model of the YF-12A. Volume 3: The MARK IVS Supersonic-Hypersonic Arbitrary Body Program, User's Manual, NASA-CR-151940.

Simsek B., Uslu S., 2019, One-Dimensional Aerodynamic Heating and Ablation Prediction, *Journal of Aerospace Engineering*, Vol.32 Issue 4.

William M.B. Jr., Katherine A.C.,1961, Free-flight aerodynamic heating data to Mach number 10.4 for a modified von Karman nosed body, NASA TN D-889.

Wing L.D., 1971, Tangent ogive nose aerodynamic heating program: NQLDW019T, NASA-TM-X-65540.

Yang G., Duan Y., Liu C., Cai J., 2014, Approximate Prediction for Aerodynamic Heating and Design for Leading-edge Bluntness on Hypersonic Vehicles. AIAA Paper 2014-1393, AIAA, Reston, VA.

Dr. Buğra ŞİMŞEK is currently a lead engineer at ROKETSAN A.Ş. He received his major and minor BSc degrees in Mechanical Engineering and Materials and Metallurgical Engineering from Middle East Technical University in 2009, respectively. He obtained his MSc degree from the Mechanical Engineering Department of Middle East Technical University in 2013. His MSc thesis involved research on missile nose heating and ablation. He received his PhD degree from TOBB University of Economics and Technology under the supervision of Assistant Professor Sıtkı USLU in December 2019. His PhD studies are related to aerodynamic heating and ablation including investigation of effects of transition from laminar to turbulent and relaminarization of the flow. Dr. ŞİMŞEK works in thermal and structural design of missiles at ROKETSAN A.Ş. since 2009. Main research areas; aerodynamic heating, thermal protection systems, nose cone ablation and thermal management.

Dr. Sıtkı USLU is assistant professor in the Department of Mechanical Engineering at TOBB University of Economics and Technology (TOBB ETU), Ankara, Turkey. Dr. USLU has obtained his first degree in mechanical engineering at Uludağ University in 1983, Bursa - Turkey. He then received his MSc degree in mechanical engineering in 1986 from Middle East Technical University, Ankara. Dr. USLU did his PhD at Imperial College London in 1993. He worked as a postdoc researcher at Imperial College in a EU Project and another year at Computational Dynamics (STAR-CD) before moving to Germany in 1995 to work in the Internal Combustion Engines research lab at Daimler Benz AG, Stuttgart - Germany. He worked as a senior CFD and combustion research engineer at Daimler Benz between 1995 to 2001. After that he moved to MTU Aero Engines in Munich and worked in the Combustion Chamber Design Group as an R&D engineer between 2001-2008. Dr. USLU has been working as a faculty staff in the Department of Mechanical Engineering at TOBB ETU since 2008 teaching Thermo-Fluid Sciences and doing research in Propulsion Systems. Dr. USLU leads the CSL (Combustion Systems Lab) at TOBB ETU that is mainly involved in research on Gas Turbine Combustion Chamber and Internal Combustion Engines. The CSL lab has participated in several national research projects and as well as EU technology projects also.

Dr. Mehmet Ali AK is a manager in ROKETSAN. He is graduated from Mechanical Engineering Department of Middle East Technical University in 1993. He obtained his MSc and PhD degrees from the same department in 1995 and 2001, respectively. He worked as lead researcher in TUBITAK SAGE for 19 years and executive designer in TUSAŞ TEI for a year. He is working in ROKETSAN A.Ş. since 2012 and today he is manager of Department of Space Systems. His main research areas; computational fluid dynamics, turbulent reactive flows, heat transfer, aerothermodynamics, numerical gas dynamics, propulsion systems and system engineering.